Sodium Cation Affinities of MALDI Matrices Determined by Guided Ion Beam Tandem Mass Spectrometry: Application to Benzoic Acid Derivatives†

S. D. M. Chinthaka, Y. Chu, N. S. Rannulu, and M. T. Rodgers*

Department of Chemistry, Wayne State University, Detroit, Michigan 48202

Received: August 19, 2005; In Final Form: November 11, 2005

Threshold collision-induced dissociation of $Na^+(x\text{BA})$ complexes with Xe is studied using guided ion beam mass spectrometry. The *x*BA ligands studied include benzoic acid and all of the mono- and dihydroxy-substituted benzoic acids: 2-, 3-, and 4-hydroxybenzoic acid and 2,3-, 2,4-, 2,5-, 2,6-, 3,4-, and 3,5-dihydroxybenzoic acid. In all cases, the primary product corresponds to endothermic loss of the intact *x*BA ligand. The cross section thresholds are interpreted to yield 0 and 298 K bond dissociation energies (BDEs) for $Na^+-x\text{BA}$ after accounting for the effects of multiple ion−neutral collisions, internal and kinetic energy distributions of the reactants, and dissociation lifetimes. Density functional theory calculations at the B3LYP/6-31G* level of theory are used to determine the structures of these complexes and provide the molecular constants necessary for the thermodynamic analysis of the experimental data. Theoretical BDEs are determined at the B3LYP/6-311+G(2d,2p) and MP2(full)/6-311+G(2d,2p) levels using the B3LYP/6-31G* optimized geometries. The trends in the measured BDEs suggest two very different binding modes for the $Na^+(x\text{BA})$ complexes, while theory finds four. In general, the most stable binding conformation involves the formation of a six-membered chelation ring via interaction with the carbonyl and 2-hydroxyl oxygen atoms. The ground state geometries of the $Na^+(x\text{BA})$ complexes in which the ligand does not possess a 2-hydroxyl group generally involve binding of Na^+ to either the carbonyl oxygen atom or to both oxygen atoms of the carboxylic acid group. These binding modes tend to be competitive because the enhancement in binding associated with the chelation interactions in the latter is mediated by steric repulsion between the hydroxyl and ortho hydrogen atoms. When possible, hydrogen bonding interactions with the ring hydroxyl group(s) enhance the stability of these complexes. The agreement between the theoretical and experimental BDEs is quite good for B3LYP and somewhat less satisfactory for MP2(full).

Introduction

Matrix assisted laser desorption ionization (MALDI) has become a versatile and increasingly popular ionization method for mass spectrometry (MS) analyses. MALDI is most often employed for the characterization of nonvolatile biological molecules, for example, proteins, carbohydrates, and nucleic acids. The direct analysis of synthetic polymers via MALDI MS is also of significant interest[1−5] for the characterization of the molecular mass distribution[6−8] and end group analyses.[9−11] MALDI is also used to characterize other types of macromolecules such as dendrimers.[12] Although MALDI has seen widespread use for the successful analysis of a wide variety of species, the ionization processes that occur in MALDI are very complex and are not fully understood. The ionization processes have been shown to be relatively independent of the matrix, solvent composition, solution pH, and analyte acid−base properties. Cationization, protonation, deprotonation, and electron transfer are all major ionization processes that occur in MALDI. Therefore, fundamental thermochemical properties (i.e., proton affinities, acidities, electron affinities, and cations affinities) of MALDI matrices and analytes are needed for a better understanding of the ionization processes that occur in MALDI. Examination of proton transfer processes and the determination of the proton affinities and basicities of MALDI matrices is currently being pursued in several research groups.[13−22] The sodium ion affinities and basicities of a variety of MALDI matrices have also been measured and calculated.[23,24] Qualitative studies of cationization processes have also been reported in the literature.[25−29]

Cationization mainly occurs due to the presence of alkali metal cations, for example, Na^+ and K^+. These metal cations are believed to come from impurities in the sample and glassware or from the processes employed to extract the analyte from its native environment.[30] In other cases, these ions are deliberately added to enhance the quality of the mass spectra.[31,32] The presence of even trace amounts of alkali metal cation salts in MALDI samples can lead to a considerable decrease in the sensitivity of the analysis. Fragmentation of the analyte molecules is also influenced by alkali metal cations. In general, the extent of fragmentation is greatest for small, high-binding-affinity cations.[33,34] However, derivatization by alkali metal cations may increase the volatility of analytes, leading to higher sensitivity, and under such conditions, cationization is unavoidable. In MALDI, the matrix functions as a mediator to provide a controllable amount of energy to facilitate vaporization and ionization of the analyte. The presence of both protonated species and alkali metal cation adducts can lead to complications in the identification of mixtures of compounds.[30] These complications can partially be alleviated by adding cation suppression agents. The alkali metal cation affinities of the analyte and potential matrices are major criteria for selecting an appropriate matrix for a particular analyte. When the cation affinity of the

† Part of the special issue "William Hase Festschrift".

10.1021/jp054698k CCC: $33.50
Published on Web 12/22/2005

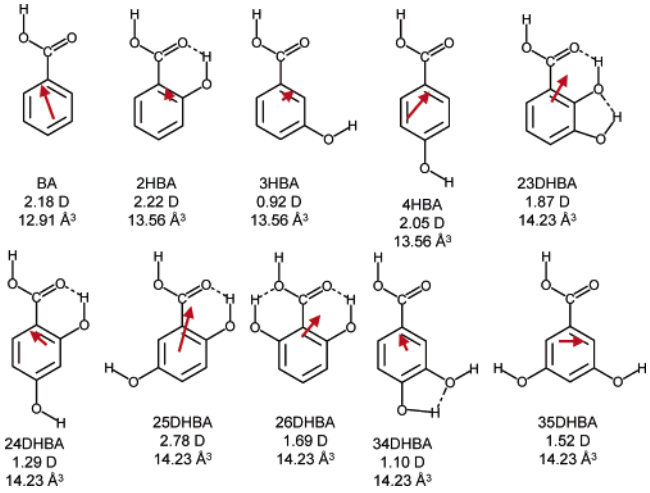

Figure 1. Structures of the *x*BA ligands. Properly scaled dipole moments (in D) are shown as arrows. The dipole moments are taken from theoretical calculations performed here. Estimated polarizabilities (in Å^3) are also shown.[46]

matrix is greater than that of the analyte, the mass spectra tend to be less complicated.[31] However, alkali metal cationization of the matrix can suppress the assistance of ionization by the matrix by blocking proton transfer ionization pathways. Alkali metal cation adducts are generally formed in one of two different ways: cationization may occur within the sample matrix and the matrix or analyte molecules are then desorbed as alkali metal cation adducts, or cationization may occur via association of the cation and matrix or analyte molecules in the gas phase. The latter process is believed to be dominant for adduct formation. Gas phase cationization is a relatively controllable process, which can be employed to optimize MALDI analyses, if the appropriate thermochemical and kinetic information is available. Therefore, the determination of the thermodynamic properties of MALDI matrices associated with alkali metal cations is important for the future understanding of the ionization processes that occur in MALDI and the optimization of MALDI for analytical analyses.

In this study, we determine the sodium cation affinities (GNa^+A's), gas phase sodium basicities (GNa^+B's), and stable binding conformations of Na^+ to benzoic acid and all of its mono- and dihydroxy-substituted derivatives. These ligands were chosen because several are widely used as MALDI matrices.[35−45] These molecules are also used as building block materials for other MALDI matrices and drug design. In this study, we use guided ion beam tandem mass spectrometry to collisionally excite complexes of Na^+ bound to 10 different benzoic acid derivatives: benzoic acid (BA), 2-hydroxybenzoic acid (2HBA), 3-hydroxybenzoic acid (3HBA), 4-hydroxybenzoic acid (4HBA), 2,3-dihydroxybenzoic acid (23DHBA), 2,4-dihydroxybenzoic acid (24DHBA), 2,5-dihydroxybenzoic acid (25DHBA), 2,6-dihydroxybenzoic acid (26DHBA), 3,4-dihydroxybenzoic acid (34DHBA), and 3,5-dihydroxybenzoic acid (35DHBA). The structures of the ground state conformations of the *x*BA matrices along with their calculated dipole moments (determined here) and estimated polarizabilities[46] are shown in Figure 1. The kinetic energy dependent cross sections for the collision-induced dissociation (CID) processes are analyzed using methods developed previously.[47,48] The internal and translational energy distributions of the reactants, multiple ion−neutral collisions, and the kinetics of unimolecular dissociation are explicitly included in the analysis. Bond dissociation energies (BDEs) of 10 Na^+(*x*BA) complexes are derived and compared with values determined from ab initio and density functional theory. Comparison is also made to the literature values reported for the Na^+(25DHBA) complex.[23,24]

Experimental Section

General Procedures. Cross sections for collision-induced dissociation (CID) of Na^+(*x*BA) with Xe, where *x*BA = BA, 2HBA, 3HBA, 4HBA, 23DHBA, 24DHBA, 25DHBA, 26DHBA, 34DHBA, and 35DHBA, are measured as a function of kinetic energy using a guided ion beam tandem mass spectrometer that has been described in detail previously.[49] Sodium ions are generated by glow discharge via Ar^+ sputtering of a tantalum or iron boat containing sodium metal operated at ~2−4 kV and ~15−30 mA. The Na^+(*x*BA) complexes are formed by condensation of Na^+ and the neutral *x*BA ligand in a 1.2 m long flow tube operating at a pressure of 0.5−0.7 Torr. The *x*BA ligands are introduced by thermal vaporization of solid samples. The Na^+(*x*BA) complexes are collisionally stabilized and thermalized by greater than 10^5 collisions with the He and Ar bath gases, such that ions emerging from the source region have internal energies that are well described by a Maxwell−Boltzmann distribution of rovibrational states at room temperature. The ions are effusively sampled, focused, accelerated, and focused into a magnetic sector momentum analyzer for reactant ion selection. Mass-selected ions are decelerated to a desired kinetic energy and focused into an octopole ion guide. The octopole passes through a static gas cell containing Xe at low pressure (~0.05−0.20 mTorr) to ensure that multiple ion−neutral collisions are improbable. The octopole ion guide acts as an efficient radial trap for ions such that scattered reactant and product ions are not lost as they drift toward the end of the octopole.[50−52] Product and unreacted beam ions are focused into a quadrupole mass filter for mass analysis and subsequently detected with a secondary electron scintillation detector (Daly detector) and standard pulse counting techniques.

Data Handling. Measured ion intensities are converted to absolute cross sections using a Beer's law analysis as described previously.[48] Absolute uncertainties in the cross section magnitudes are estimated to be ±20%, which are derived largely from errors in the pressure measurement and length of the interaction region. Relative uncertainties are approximately ±5%.

Ion kinetic energies in the laboratory frame, E_{lab}, are converted to energies in the center-of-mass frame, E_{CM}, using the formula $E_{CM} = E_{lab}m/(m + M)$, where M and m are the masses of the ionic and neutral reactants, respectively. All energies reported below are in the center-of-mass frame unless otherwise noted. The absolute zero and distribution of the ion kinetic energies are determined using the octopole ion guide as a retarding potential analyzer as previously described.[48] The distribution of ion kinetic energies is nearly Gaussian with a full width at half-maximum (fwhm) between 0.2 and 0.4 eV (lab) for these experiments. The uncertainty in the absolute energy scale is ±0.05 eV (lab).

Because multiple ion−neutral collisions can influence the shape of CID cross sections, and the threshold regions are most sensitive to these effects, each CID cross section was measured twice at three nominal Xe pressures (0.05, 0.10, and 0.20 mTorr). Data free from pressure effects are obtained by extrapolating to zero reactant pressure, as previously described.[53] The zero-pressure-extrapolated cross sections subjected to thermochemical analysis are therefore the result of single bimolecular encounters.

Theoretical Calculations. To obtain model structures, vibrational frequencies, rotational constants, and energetics for

the neutral *x*BA ligands and their complexes to Na^+, ab initio and density functional theory calculations were performed using Gaussian 98.[54] Geometry optimizations were performed at the B3LYP/6-31G* level of theory. Vibrational analyses of the geometry-optimized structures were performed to determine the vibrational frequencies of the optimized species. The vibrational frequencies thus calculated were prescaled by a factor of 0.9804 for zero point energy corrections, thermal energy adjustments, and modeling of the experimental data.[55] The prescaled vibrational frequencies are listed in the Supporting Information, Table 1S. The rotational constants of the ground state conformations are provided in the Supporting Information, Table 2S. Single point energy calculations were performed at the B3LYP/6-311+G(2d,2p) and MP2(full)/6-311+G(2d,2p) levels of theory using the B3LYP/6-31G* optimized geometries. Zero point energy (ZPE) and basis set superposition error (BSSE) corrections were included in the calculation of theoretical BDEs.

As a result of the multiple orientations possible for the carboxylic acid moiety and hydroxyl group(s), as well as the multiple favorable Na^+ binding sites to these *x*BA ligands, numerous low-energy conformations of these species are possible. Therefore, we carefully consider all possible conformations of the *x*BA ligands (i.e., 2 for BA, 4 for 4HBA, 8 for 2HBA, 3HBA, 26DHBA, and 35DHBA, and 16 for 23DHBA, 24DHBA, 25DHBA, and 34DHBA) and numerous conformations of the Na^+(*x*BA) complexes (i.e., those that are likely to exhibit strong binding) to determine their relative stabilities and the ground state conformations of these species. In several cases, transition states (TSs) between various conformations of the neutral *x*BA ligands and the Na^+(*x*BA) complexes are also calculated to determine the barriers for interconversion to establish whether such conformational changes can occur under the experimental conditions employed.

Thermochemical Analysis. The threshold regions of the CID cross sections are modeled using an empirical threshold energy law, eq 1

$$\sigma(E) = \sigma_0 \sum_i g_i (E + E_i - E_0)^n / E \qquad (1)$$

where σ_0 is an energy independent scaling factor, E is the relative translational energy of the reactants, E_0 is the threshold for reaction of the ground electronic and rovibrational state, and n is an adjustable parameter that describes the efficiency of kinetic to internal energy transfer.[56] The summation is over the rovibrational states of the reactant ions, i, where E_i is the excitation energy of each rovibrational state and g_i is the relative population of each state ($\sum g_i = 1$). The relative reactivity of all rovibrational states, as reflected by σ_0 and n, is assumed to be equivalent.

The Beyer−Swinehart algorithm[57−59] is used to evaluate the density of the rovibrational states, i, and the relative populations, g_i, are calculated by a Maxwell−Boltzmann distribution at 298 K, the internal temperature of the reactants. The average internal energies of the ground state conformations of the neutral *x*BA ligands and Na^+(*x*BA) complexes are also included in the Supporting Information, Table 1S. To account for the inaccuracies in the computed frequencies, we have increased and decreased the prescaled frequencies by 10%. This encompasses the range of scale factors needed to bring calculated frequencies into agreement with experimentally determined frequencies.[60,61] The corresponding change in the average vibrational energy is taken to be an estimate of one standard deviation of the uncertainty in the vibrational energy (Supporting Information, Table 1S).

Statistical theories for unimolecular dissociation, specifically the Rice−Ramsperger−Kassel−Marcus (RRKM) theory, of the collisionally activated ions are also included in eq 1 to account for the possibility that these ions may not have undergone dissociation prior to arriving at the detector ($\sim 10^{-4}$ s), as described in detail elsewhere.[47,62] In our analysis, we assume that the TS is loose and product-like because the interaction between Na^+ and the *x*BA ligand is largely electrostatic. The best model for the TS of such electrostatically bound complexes is a loose phase space limit (PSL) model located at the centrifugal barrier for the interaction of Na^+ with *x*BA, as described in detail elseware.[47] The parameters appropriate for the PSL model TS are the frequencies and rotational constants of the products. The rovibrational frequencies appropriate for the energized molecules and the TSs leading to dissociation are given in the Supporting Information, Tables 1S and 2S.

The model represented by eq 1 is expected to be appropriate for translationally driven reactions[63] and has been found to reproduce CID cross sections well. The model of eq 1 is convoluted with the kinetic energy distributions of both the reactant Na^+(*x*BA) complex and neutral Xe atom, and a nonlinear least-squares analysis of the data is performed to give optimized values for the parameters σ_0, E_0, and n. The error associated with the measurement of E_0 is estimated from the range of threshold values determined for the eight zero-pressure-extrapolated data sets, variations associated with uncertainties in the vibrational frequencies (scaling as discussed above), and the error in the absolute energy scale, 0.05 eV (lab). For analyses that include the RRKM lifetime analysis, the uncertainties in the reported E_0(PSL) values also include the effects of increasing and decreasing the assumed time available for dissociation ($\sim 10^{-4}$ s) by a factor of 2.

Equation 1 explicitly includes the internal energy of the reactant ion, E_i. All energy available is treated statistically because the internal energy of the reactants is redistributed throughout the accessible rovibrational energy states of the complex upon collision with Xe. The threshold for dissociation is by definition the minimum energy required leading to dissociation and thus corresponds to the formation of products with no internal excitation. The assumption that products formed at threshold have an internal temperature of 0 K has been tested for a variety of systems.[47,49,53,56,62] It has also been shown that treating all energy of the ion (vibrational, rotational, and translational) as capable of coupling into the dissociation coordinate leads to accurate thermochemistry.[47,49,53,56,62] The threshold energies, E_0(PSL), obtained from these analyses can be equated to 0 K BDEs by assuming that E_0(PSL) represents the energy difference between reactants and products at 0 K.[64] This assumption requires that there are no activation barriers in excess of the endothermicity of dissociation. This is generally true for ion−molecule reactions[65] and should be valid for the simple noncovalent bond fission reactions examined here.[66]

Results

Cross Sections for Collision-Induced Dissociation. Experimental cross sections were obtained for the interaction of Xe with 10 Na^+(*x*BA) complexes, where *x*BA = BA, 2HBA, 3HBA, 4HBA, 23DHBA, 24DHBA, 25DHBA, 26DHBA, 34DHBA, and 35DHBA. Figure 2 shows representative data for the Na^+(25DHBA) complex. The other Na^+(*x*BA) complexes exhibit similar behavior and are included in the Supporting Information, Figure 1S. Over the collision energy range examined, 0−7.5 eV, two types of processes are observed: loss of the intact *x*BA ligand and ligand exchange with Xe. The most

TABLE 1: Modeling Parameters of eq 1 and Entropies of Activation at 1000 K of $Na^+(xBA)$[a]

reactant cation	σ_0[b]	n[b]	E_0[c] (eV)	E_0(PSL)[b] (eV)	kinetic shift (eV)	$\Delta S^{\ddagger}$(PSL)[b] (J/(K mol))
Na^+(BA)	13.4 (0.7)	1.4 (0.1)	1.49 (0.04)	1.34 (0.04)	0.15	20 (2)
Na^+(2HBA)	2.7 (0.1)	1.1 (0.1)	1.75 (0.03)	1.48 (0.04)	0.27	29 (1)
Na^+(3HBA)	2.4 (0.2)	1.2 (0.1)	1.57 (0.03)	1.36 (0.03)	0.21	19 (1)
Na^+(4HBA)	1.4 (0.2)	1.3 (0.1)	1.56 (0.06)	1.36 (0.05)	0.20	21 (1)
Na^+(23DHBA)	8.3 (0.5)	1.4 (0.1)	1.88 (0.05)	1.50 (0.16)	0.38	21 (1)
Na^+(24DHBA)	2.7 (0.1)	1.2 (0.1)	1.86 (0.06)	1.50 (0.04)	0.36	17 (2)
Na^+(25DHBA)	15.7 (1.4)	1.3 (0.1)	1.90 (0.06)	1.50 (0.05)	0.40	19 (1)
Na^+(26DHBA)	2.5 (0.4)	1.5 (0.1)	1.80 (0.03)	1.50 (0.03)	0.30	29 (1)
Na^+(34DHBA)	2.6 (0.3)	1.3 (0.1)	1.78 (0.03)	1.42 (0.03)	0.36	19 (1)
Na^+(35DHBA)	2.4 (0.6)	1.3 (0.1)	1.70 (0.10)	1.41 (0.07)	0.31	34 (1)

[a] Uncertainties are listed in parentheses. [b] Average values for the loose PSL transition state. [c] No RRKM analysis.

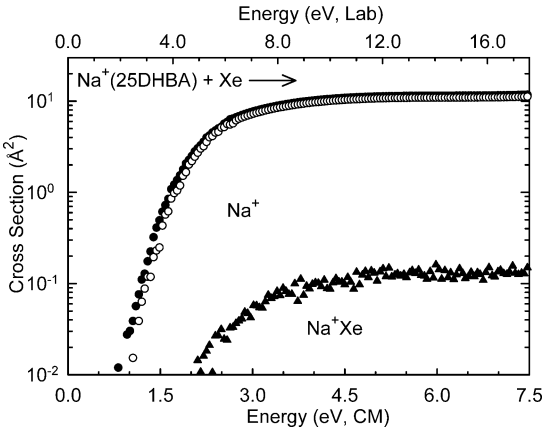

Figure 2. Cross section for collision-induced dissociation of Na^+-(25DHBA) with Xe as a function of kinetic energy in the center-of-mass frame (lower *x*-axis) and the laboratory frame (upper *x*-axis). Data for the Na^+ product are shown for a Xe pressure of ~0.2 mTorr (●) and extrapolated to zero (○).

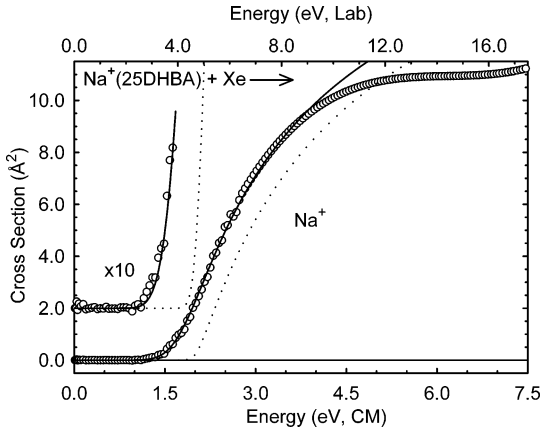

Figure 3. Zero-pressure-extrapolated cross section for collision-induced dissociation of Na^+(25DHBA) with Xe in the threshold region as a function of kinetic energy in the center-of-mass frame (lower *x*-axis) and the laboratory frame (upper *x*-axis). The solid line shows the best fit to the data using the model of eq 1 convoluted over the neutral and ion kinetic and internal energy distributions. The dotted line shows the model cross sections in the absence of experimental kinetic energy broadening for reactants with an internal temperature of 0 K.

favorable process for all complexes is loss of the intact *x*BA ligand in CID reactions 2.

$$Na^+(xBA) + Xe \rightarrow Na^+ + xBA + Xe \qquad (2)$$

Ligand exchange processes to form Na^+Xe are also observed as very minor reaction pathways in several of the systems examined here, reaction 3.

$$Na^+(xBA) + Xe \rightarrow Na^+Xe + xBA \qquad (3)$$

It is likely that this process occurs for all $Na^+(xBA)$ complexes but that the signal-to-noise ratio in the other experiments was not sufficient to differentiate the Na^+Xe product from background noise. When observed, the cross sections for ligand exchange are approximately 2 orders of magnitude smaller than those for the primary CID pathway.

Threshold Analysis. The model of eq 1 was used to analyze the thresholds for CID reactions 2 in 10 $Na^+(xBA)$ systems. The results of these analyses are provided in Table 1, and representative results for the Na^+(25DHBA) complex are shown in Figure 3. The analyses for the other $Na^+(xBA)$ complexes are shown in the Supporting Information, Figure 2S. In all cases, the experimental cross sections are accurately reproduced using a loose PSL TS model.[47] Previous work has shown that this model provides the most accurate assessment of the kinetic shifts for CID of electrostatically bound ion−molecule complexes.[47,67] Good reproduction of the experimental data is obtained over energy ranges exceeding 2.5 eV and cross section magnitudes of at least a factor of 100. Table 1 also includes threshold values, E_0, obtained without inclusion of the RRKM lifetime analysis. Comparison of these results with the E_0(PSL) values provides a measure of the kinetic shift associated with the finite experimental time window, which should correlate with the density of states at threshold. The kinetic shifts vary between 0.15 and 0.40 eV for these systems. The kinetic shift is the smallest for the Na^+(BA) complex, increases for the Na^+(HBA) complexes, and is largest for the Na^+(DHBA) complexes. This trend is easily understood because the number of vibrational modes available to the complexes increases in that order: 42 for Na^+(BA), 45 for the Na^+(HBA) complexes, and 48 for the Na^+(DHBA) complexes. Among the Na^+(HBA) complexes, the kinetic shifts are similar for Na^+(3HBA) and Na^+(4HBA) and larger for Na^+(2HBA) as expected because this parallels the measured BDEs. Among the Na^+(DHBA) complexes, the trend is not quite as simple but roughly parallels the measured BDEs.

The entropy of activation, $\Delta S^{\ddagger}$, is a measure of the looseness of the TS and also a reflection of the complexity of the system. $\Delta S^{\ddagger}$ is largely determined by the molecular parameters used to model the energized molecule and TS for dissociation but also depends on the threshold energy. The $\Delta S^{\ddagger}$(PSL) values at 1000 K are listed in Table 1 and vary from 17 to 34 J/(K mol) across these systems.

Theoretical Results. Theoretical structures for the neutral *x*BA ligands, $Na^+(xBA)$ complexes, and in limited cases TSs for interconversion of various conformers of these species as well as theoretical BDEs for the $Na^+(xBA)$ complexes were calculated as described in the Theoretical Calculations section.

Neutral *x*BA Ligands. Schematic diagrams of the ground state conformations determined for the *x*BA ligands and their calculated dipole moments are shown in Figure 1. In all cases,

the ground state structures are nearly planar with the hydrogen atom of the carboxylic acid moiety oriented away from the phenyl ring. Intramolecular hydrogen bonds provide enhanced stability and are present in the ground state conformations in all cases where the substituents (carboxylic acid moiety and hydroxyl substituent(s)) occupy adjacent sites on the phenyl ring. The geometry-optimized structures, calculated dipole moments, and relative stabilities (including ZPE corrections) of all stable conformations of the neutral *x*BA ligands are provided in the Supporting Information, Figure 3S. In cases where two substituents occupy adjacent sites on the phenyl ring (i.e., 2HBA, 23DHBA, 24DHBA, 25DHBA, 26DHBA, and 34DHBA), fewer stable structures than the maximum possible are found because conformations in which the hydroxyl hydrogen atoms of the adjacent substituents are oriented toward each other are unfavorable. Such conformations either never converged or more often converged to one of the more favorable conformations via rotation of one of the hydroxyl groups.

Insight into the factors that lead to stability in these *x*BA ligands can be obtained by comparing the various conformations and their relative stabilities (Supporting Information, Figure 3S). As discussed above, the hydroxyl group of the carboxylic acid moiety is oriented away from the phenyl ring in the ground state conformations of all of the *x*BA ligands. Alternatively, the hydroxyl group of the carboxylic acid moiety could point toward the phenyl ring. The latter conformations are much less favorable as a result of steric repulsion between the hydrogen atom of the carboxylic acid moiety and the ortho hydrogen atom of the phenyl ring, which causes the carboxylic acid moiety to rotate out of the plane. This leads to a reduction in the stability gained via resonance delocalization of the carbonyl π electrons with those of the aromatic ring and costs ~20−27 kJ/mol as estimated from the relative stabilities of the corresponding conformers of the various neutral *x*BA ligands. Intramolecular hydrogen bonds clearly provide enhanced stability to these *x*BA ligands. Hydrogen bonds between the carbonyl oxygen atom and the hydrogen atom of the 2-hydroxyl group, when present, are the most favorable. Such hydrogen bonding leads to 23.4 kJ/mol stabilization in 2HBA, whereas the stabilization gained in the dihydroxy-substituted systems (i.e., 23DHBA, 24DHBA, 25DHBA, and 26DHBA) is significantly larger, 41.6−59.1 kJ/mol. It is unknown why so much less stabilization is gained upon formation of this hydrogen bond in 2HBA as compared to the DHBA ligands. Clearly, other factors play a role; for example, the dipole moments of the various conformers, but no systematic differences in the dipole moments of the corresponding conformers are found. Hydrogen bonds between the hydroxyl oxygen atom of the carboxylic moiety and the hydrogen atom of the 2-hydroxyl group when present are the next most favorable. Such hydrogen bonding leads to 20.9−31.6 kJ/mol stabilization. Hydrogen bonds between adjacent hydroxyl groups when present (i.e., 23DHBA and 34DHBA) are the next most favorable, providing 12.4−22.4 kJ/mol stabilization. The least favorable hydrogen bonding interactions occur between the hydrogen atom of the carboxylic acid moiety and the oxygen atom of the 2-hydroxyl group when present, which provide 0.5−6.2 kJ/mol stabilization. The most likely reason for the small differences in stability upon breaking of the latter hydrogen bonds is that conformers possessing such hydrogen bonds exhibit very large dipole moments. In all cases except 26DHBA, conformers engaging in such hydrogen bonds are much less stable (by >30 kJ/mol) than the ground state conformations and therefore are unimportant for the neutral species. However, such conformations are likely to bind strongly to Na^+ and in fact are among the low-energy conformers of all of the Na^+(*x*BA) complexes that could engage in such hydrogen bonds, (i.e., 2HBA, 23DHBA, 24DHBA, 25DHBA, and 26DHBA).

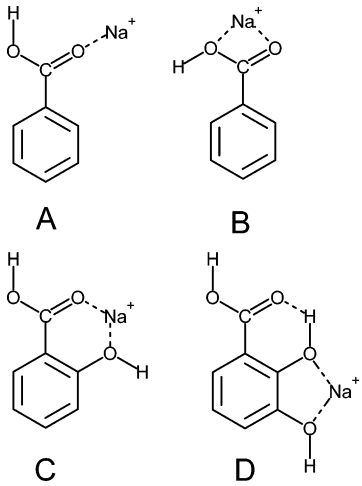

Figure 4. Energetically favorable stable binding modes of Na^+ to the *x*BA ligands.

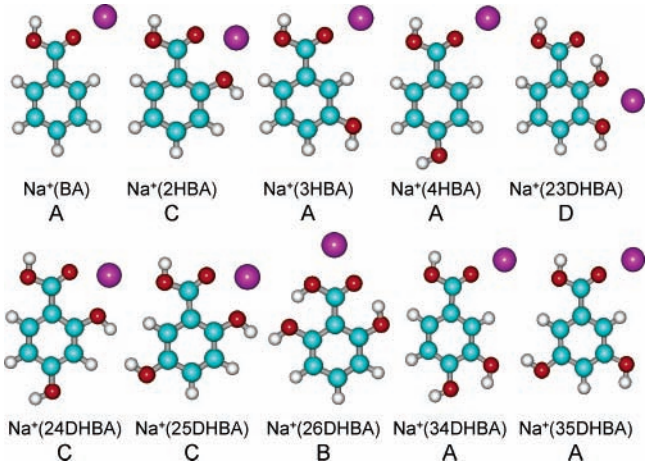

Figure 5. Ground state geometries of the Na^+(*x*BA) complexes optimized at the B3LYP/6-31G* level of theory.

Na^+(*x*BA) Complexes. Four distinct favorable Na^+ binding modes to the *x*BA ligands are found, as shown schematically for several of the *x*BA ligands in Figure 4. Clearly, stable binding geometries in which Na^+ interacts with a single hydroxyl oxygen atom also exist. However, the binding in such complexes is much weaker than that of the four binding modes shown in Figure 4. For the Na^+(BA) complex, binding to the hydroxyl oxygen atom of the carboxylic acid moiety is less favorable than the ground state A conformer by 48.7 kJ/mol. For the Na^+(3HBA) complex, binding to the 3-hydroxyl oxygen atom is less favorable than the ground state A conformer by 41.3 kJ/mol. Similar or larger differences in stability are expected for the analogous binding modes to the other *x*BA ligands, and therefore, such binding conformations were not considered further.

The ground state conformations of all 10 Na^+(*x*BA) complexes are shown in Figure 5. In all cases except BA, the neutral *x*BA ligand undergoes a change in conformation to achieve optimal binding to Na^+ (compare Figures 1 and 5). All low-energy conformations of the Na^+(*x*BA) complexes that might be expected to be populated under our experimental conditions (i.e., 298 K internal energy distribution, and therefore within 10 kJ/mol of the ground state structures) and their relative

TABLE 2: Measured and Calculated Enthalpies of Sodium Ion Binding to *x*BA at 0 K in kJ/mol

	experiment			theory					
				MP2[b]			B3LYP[c]		
Na^+(*x*BA)	TCID	binding mode	μ[a] (D)	D_e	D_0[d]	$D_{0,BSSE}$[e]	D_e	D_0[d]	$D_{0,BSSE}$[e]
Na^+(BA)	130.1 (4.0)	A	2.50	126.8	124.0	116.4	138.1	135.4	132.8
		B	5.30	120.3	119.0	110.0	135.7	134.4	131.8
Na^+(2HBA)	143.3 (3.8)	C	3.32	139.5	137.3	126.8	144.5	142.3	139.0
		B	7.14	136.6	136.2	127.2	141.5	141.0	138.3
Na^+(3HBA)	131.2 (3.1)	A1	3.71	129.8	127.3	120.0	140.3	137.8	135.3
		A2	3.21	126.6	124.3	117.5	137.5	135.2	132.7
		B1	6.24	129.1	127.8	119.6	136.5	135.2	132.6
		B2	6.59	128.8	127.7	119.6	136.2	135.1	132.6
		B3	4.04	126.3	125.9	117.6	134.5	134.0	131.4
		A3	2.52	125.1	122.7	115.5	136.1	133.7	131.2
		A4	1.22	119.1	116.9	109.5	130.5	128.3	125.7
		B4	4.85	121.0	119.8	117.7	128.7	127.6	125.0
Na^+(4HBA)	131.5 (4.7)	A1	3.90	132.9	129.8	122.5	146.6	143.5	140.9
		B1	5.51	133.9	132.5	124.1	144.6	143.2	140.6
		B2	6.56	132.8	131.5	123.2	143.5	142.1	139.5
		A2	2.54	130.8	127.8	120.4	144.7	141.7	139.2
Na^+(23DHBA)	145.2 (4.1)	D	3.47	150.2	149.9	139.8	152.7	152.3	149.2
		C	4.73	147.1	145.0	134.2	152.5	150.4	147.0
		B	8.19	138.1	137.5	128.8	143.6	142.9	140.2
Na^+(24DHBA)	145.3 (3.7)	C	4.43	143.2	140.7	130.3	149.4	146.8	143.5
		B1	7.19	140.8	139.9	131.1	147.0	146.1	143.3
		B2	8.38	136.6	136.0	127.2	142.8	142.1	139.4
Na^+(25DHBA)	145.4 (4.6)	C1	2.74	142.2	139.7	129.4	148.1	145.6	142.4
		C2	4.38	141.8	139.6	129.3	147.6	145.5	142.2
		B1	8.42	138.7	138.5	129.7	143.9	143.7	141.0
		B2	5.88	138.1	137.7	129.1	143.6	143.2	140.4
Na^+(26DHBA)	145.0 (3.7)	B	6.45	146.4	145.1	136.2	151.8	150.5	147.5
Na^+(34DHBA)	138.0 (3.0)	A1	5.16	135.0	132.2	124.7	146.8	144.0	141.4
		B1	4.30	133.3	132.0	121.5	144.1	142.8	140.2
		B2	6.59	134.2	133.4	124.9	143.7	142.8	140.2
		B3	7.91	132.9	132.3	123.9	142.1	141.5	138.8
		A2	3.65	129.4	126.8	119.5	141.8	139.1	136.6
		A3	1.53	123.9	121.4	114.0	138.1	135.7	133.1
Na^+(35DHBA)	136.4 (7.1)	A1	3.49	129.8	127.3	120.0	140.1	137.6	136.4
		A2	4.44	128.4	126.1	118.7	138.7	136.5	134.2
		B1	5.03	129.3	127.6	119.5	137.0	135.3	132.8
		B2	7.51	128.8	127.2	119.0	136.5	134.9	132.3
		B3	6.04	123.7	122.3	114.1	131.6	130.1	127.5
		A3	1.98	120.7	118.3	111.1	131.8	129.5	126.9
MAD					**4.5 (2.5)**	**12.2 (3.9)**			**3.5 (2.4)**

[a] Calculated dipole moment of the neutral conformer in the geometry it exists in the complex. [b] Calculated at the MP2(full)/6-311+G(2d,2p) level of theory using B3LYP/6-31G* optimized geometries and assuming that the complex dissociates to the ground state neutral conformer. [c] Calculated at the B3LYP/6-311+G(2d,2p) level of theory using B3LYP/6-31G* optimized geometries and assuming that the complex dissociates to the ground state neutral conformer. [d] Also includes ZPE corrections with frequencies scaled by 0.9804. [e] Also includes BSSE corrections.

stabilities are also provided in the Supporting Information, Figure 4S. Theoretical BDEs for the ground state and low-energy conformations of the Na^+(*x*BA) complexes calculated at the B3LYP/6-311+G(2d,2p) and MP2(full)/6-311+G(2d,-2p) levels of theory (using geometries optimized at the B3LYP/6-31G* level of theory and assuming that the complexes dissociate to produce the neutral *x*BA ligand in its ground state conformation) are summarized along with the measured values in Table 2. The calculated energies of the associated Na^+(*x*BA) complexes, Na^+, and the *x*BA ligands are provided in the Supporting Information, Tables 3S and 4S. To understand the trends in the binding of Na^+ to these *x*BA ligands, the dipole moments of the *x*BA ligands in the conformations they assume in the Na^+(*x*BA) complexes are also provided in Table 2. Comparison of these dipole moment values to those for the analogous neutral conformers shows that the dipole moment always increases upon Na^+ binding (compare Table 2 and Figure 3S of the Supporting Information).

The calculations find two favorable binding modes for Na^+ to BA. Binding of Na^+ to the ground state conformation of neutral BA occurs at the carbonyl oxygen atom (binding mode A, Figure 4). The C═O—Na^+ bond angle is very nearly linear but shifted slightly away from the hydroxyl group. An alternative binding mode is possible when the hydrogen atom of the carboxylic acid moiety is oriented toward the phenyl ring, thereby allowing Na^+ to interact with both oxygen atoms of the carboxylic acid moiety and forming a four-membered chelation ring (binding mode B, Figure 4). The relative stability of the A and B conformations of Na^+(BA) is found to depend on the level of theory employed. B3LYP calculations favor mode A over mode B by 1.0 kJ/mol, whereas MP2 calculations suggest that mode A is favored by 6.4 kJ/mol. These results suggest that a single interaction with the carbonyl oxygen atom is more favorable than chelation interactions with both oxygen atoms of the carboxylic acid moiety. At first, this result appears somewhat surprising. However, the most likely reason for the preference of binding mode A over binding mode B is that the steric repulsion between the hydrogen atom of the carboxylic acid moiety and the ortho hydrogen atom of the phenyl ring that occurs in mode B causes the carboxylic acid moiety to rotate out of the plane. This leads to a reduction in the stability gained via resonance delocalization of the carbonyl π electrons with

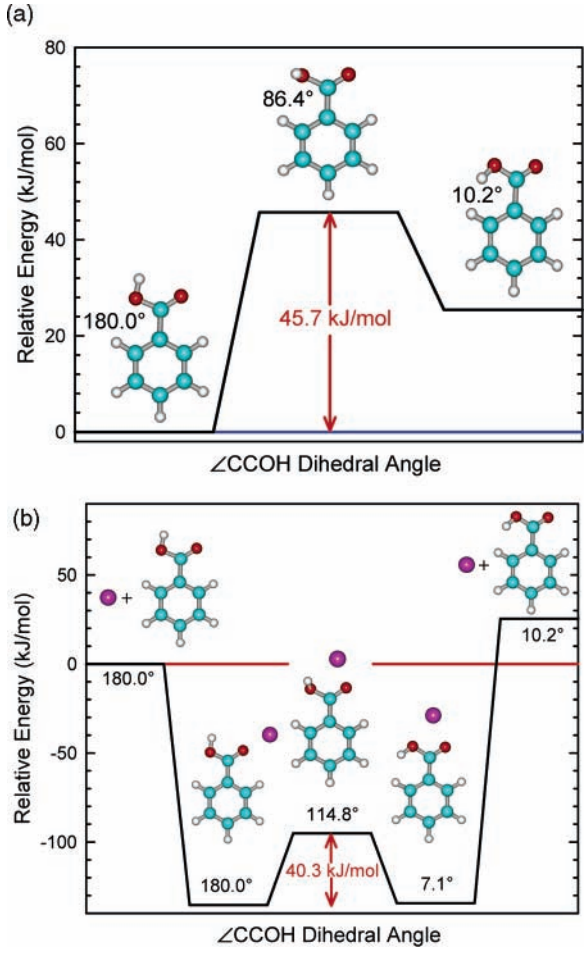

Figure 6. Reaction coordinate diagrams for the interconversion of the two stable conformers of (a) BA and (b) Na^+(BA).

those of aromatic ring and costs ~25.4 kJ/mol, as estimated from the relative stabilities of the corresponding conformers of neutral BA. Interconversion of these conformers is not feasible for neutral BA because the TS for interconversion lies 45.7 kJ/mol higher in energy than the ground state neutral conformer, almost 3 times as large as the internal energy of BA (Supporting Information, Table 1S). However, complexation to Na^+ facilitates this geometry change by providing the energy associated with complexation (135.4 kJ/mol, B3LYP excluding BSSE corrections) as well as slightly reducing the barrier to interconversion (40.3 kJ/mol) of the A and B conformers of Na^+(BA). The calculated potential energy surfaces (PESs) for these processes for BA and Na^+(BA) are provided in Figure 6.

The preference for binding mode A over binding mode B is also found for the Na^+(3HBA), Na^+(4HBA), Na^+(34DHBA), and Na^+(35DHBA) complexes for B3LYP and MP2 calculations, except for the Na^+(4HBA) complex where MP2 suggests that binding mode B is favored over binding mode A by 1.6 kJ/mol. In all of these complexes, multiple low-energy A and B type conformers are found that differ only in the relative orientations of the carboxylic acid moiety and hydroxyl groups (compare Figure 5 and Figure 4S of the Supporting Information). Although not explicitly calculated, interconversion of the A and B conformers in these latter systems should also be facile because complexation to Na^+ provides a slightly greater amount of energy than for the BA system (137.6−144.0 kJ/mol, B3LYP excluding BSSE corrections). In addition, the energy required for interconversion of the A and B type conformers of these systems should be similar to that calculated for Na^+(BA) because the hydroxyl groups are distant from the carboxylic acid moiety and therefore should not significantly impact such interconversion. Similarly, changes in the orientation(s) of the hydroxyl group(s) attached to the phenyl ring may not be feasible for the neutral *x*BA ligands because the TSs for interconversion lie ~14−25 kJ/mol higher in energy than the lower energy conformer (e.g., 13.8 kJ/mol for 3HBA and 24.9 kJ/mol for 4HBA) when no hydrogen bonds are involved and ~26−28 kJ/mol higher in energy than the lower energy conformer (e.g., 26.1 and 28.1 kJ/mol for 34DHBA) when hydrogen bonds must be broken during the change in conformation, and thus roughly equal or exceed the internal energy of the *x*BA ligands (Supporting Information, Table 1S). Similarly, changes in the orientation of the carboxylic acid moiety relative to the hydroxyl groups may not be feasible for the neutral *x*BA ligands because the TSs for interconversion lie ~26.9 kJ/mol higher in energy than the ground state conformer as estimated for 3HBA. Again, complexation to Na^+ facilitates such conformational changes by providing the energy associated with complexation, which significantly exceeds these barriers. In all other cases where binding mode B is favored over binding mode A (i.e., Na^+(2HBA), Na^+(23DHBA), Na^+(24DHBA), Na^+(25DHBA), and Na^+(26DHBA)), this preference arises as a result of hydrogen bonding interactions between the hydrogen atom of the 2-hydroxyl substituent and the carbonyl oxygen atom that help stabilize binding mode B relative to binding mode A.

The calculations find two very favorable binding modes for Na^+ to 2HBA. Binding of Na^+ to the ground state conformation of neutral 2HBA again occurs at the carbonyl oxygen atom, producing an A conformer. However, this structure does not correspond to either of the most favorable binding modes and lies 36.9 kJ/mol higher in energy than the ground state conformation. Rotation of the Na^+ bound carboxylic acid moiety by 180°, thereby breaking the original hydrogen bond and creating a new hydrogen bond between the 2-hydroxyl group and the oxygen atom of the hydroxyl group of the carboxylic acid moiety, produces a second A conformer that is slightly more stable but still lies 31.1 kJ/mol higher in energy than the ground state conformer. In contrast to that found for BA, 3HBA, 4HBA, 34DHBA, and 35DHBA, the B conformer of Na^+(2HBA) is much more stable than the A conformers. Clearly, steric repulsion between Na^+ and the hydrogen atom of the 2-hydroxyl group in the A conformers weakens the hydrogen bonding and Na^+ binding interactions, thereby destabilizing these species. For Na^+(2HBA), the B conformer lies 1.3 kJ/mol higher in energy than the ground state conformation. An alternative binding mode is possible when the 2-hydroxyl group rotates 180°, thereby breaking the original hydrogen bond and allowing Na^+ to simultaneously interact with the carbonyl oxygen atom and the 2-hydroxyl oxygen atom and forming a six-membered chelation ring (binding mode C, Figure 4). Thus, the binding geometry of Na^+ in the six-membered chelation ring is more favorable than that of the four-membered chelation ring because conformer C is more stable than conformer B even though the former requires that the hydrogen bond between the carbonyl oxygen atom and the 2-hydroxyl hydrogen atom be broken. The calculated PES for the interconversion of A, B, and C type conformers of 2HBA is provided in Figure 7. The analogous TSs for interconversion of the conformers of the Na^+(2HBA) complex are expected to be similar, or slightly smaller, and thus were not explicitly calculated here.

The preference for binding mode C over binding mode B is found for the Na^+(2HBA), Na^+(23DHBA), Na^+(24DHBA), and Na^+(25DHBA) complexes for both B3LYP and MP2 results.

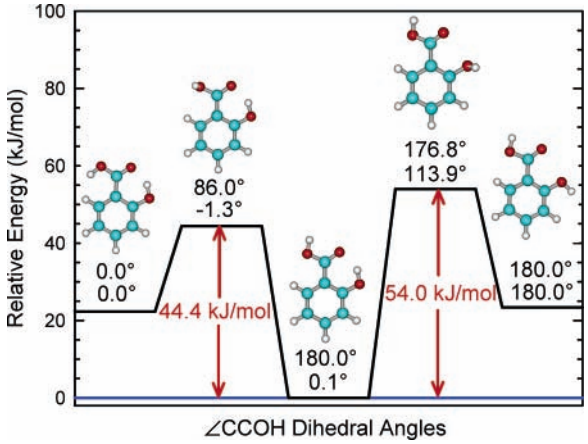

Figure 7. Reaction coordinate diagram for the interconversion of three of the low-energy conformers of 2HBA.

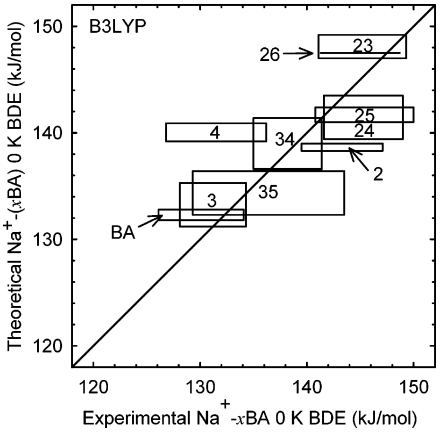

Figure 8. Theoretical B3LYP/6-311+G(2d,2p) versus experimental Na^+-xBA BDEs (in kJ/mol). All values are at 0 K and taken from Table 2. The boxes indicate the range of values that are appropriately compared. The experimental range corresponds to the measured BDE plus or minus the experimental uncertainty, while the theoretical range corresponds to the calculated BDEs for the ground and low-lying (within ~5 kJ/mol) excited state conformers. The diagonal line indicates the values for which calculated and measured BDEs are equal.

However, the B and C conformations are of very similar stability in all of the above complexes. In contrast, the C conformers of 26DHBA are significantly less stable (by ~15 kJ/mol) than the ground state B conformer. A likely reason for this difference in behavior is that in the B conformer 26DHBA is able to engage in two hydrogen bonds and the conformation of the neutral ligand exhibits a very large dipole moment, whereas the C conformer engages in only a single hydrogen bond and the conformation of the neutral ligand exhibits a much smaller dipole moment.

The calculations find a third very favorable binding mode for Na^+ to 23DHBA. In this case, Na^+ binds to both of the oxygen atoms of the adjacent hydroxyl groups and forms a five-membered chelation ring (binding mode D, Figure 4). In general, theoretical calculations show that this binding mode is less favorable than the formation of the six-membered ring (binding mode C). However, in this case, the five-membered chelation ring structure is stabilized by a hydrogen bond between the carbonyl oxygen atom and the 2-hydroxyl hydrogen atom. B3LYP calculations favor conformer D over conformer C by 2.2 kJ/mol, whereas MP2 calculations suggest that conformer D is favored by 5.6 kJ/mol. Binding via such a five-membered chelation ring is also possible in 34DHBA. However, without the enhanced stability associated with the hydrogen bonding that occurs in Na^+(23DHBA), conformer D is not nearly as stable as the various A and B conformers of this complex. B3LYP calculations find that conformer D of Na^+(34DHBA) lies 15.1 kJ/mol above the ground state A conformer. In contrast, MP2 calculations suggest that conformer D is somewhat more stable and only lies 5.5 kJ/mol above the ground state conformer.

Conversion from 0 to 298 K. To allow comparison to literature values and commonly used experimental conditions, we convert the 0 K BDEs determined here to 298 K bond enthalpies and free energies. The enthalpy and entropy conversions are calculated using standard formulas and the vibrational and rotational constants determined for the B3LYP/6-31G* optimized geometries given in the Supporting Information, Tables 1S and 2S. Table 3 shows 0 and 298 K enthalpy, free energy, and enthalpic and entropic corrections for all of the systems. Uncertainties in the enthalpic and entropic corrections are determined by 10% variation in the molecular constants. For the Na^+(*x*BA) complexes, where the Na^+-xBA frequencies are very low and may not be adequately described by theory, the listed uncertainties also include changing the three metal−ligand frequencies by a factor of 2. This provides a conservative estimate of the computational errors in these low-frequency modes and is the dominant source of the uncertainties listed here.

Discussion

Comparison of Theoretical and Experimental Results. The experimentally measured BDEs of the Na^+(*x*BA) complexes at 0 K are summarized in Table 2. Also listed in Table 2 are the corresponding theoretical BDEs calculated at the B3LYP/6-311+G(2d,2p) and MP2(full)/6-311+G(2d,2p) levels of theory. The agreement between B3LYP theory and experiment is illustrated in Figure 8, while the MP2 theory and measured BDEs are compared in Figure 9. As seen in Table 2, our theoretical results suggest that multiple low-energy conformers

TABLE 3: Enthalpies and Free Energies of Sodium Ion Binding to *x*BA at 298 K in kJ/mol[a]

Na^+(*x*BA)	ΔH_0	$\Delta H_0{}^b$	$\Delta H_{298} - \Delta H_0{}^b$	ΔH_{298}	$\Delta H_{298}{}^b$	$T\Delta S_{298}{}^b$	ΔG_{298}	$\Delta G_{298}{}^b$
Na^+(BA)	130.1 (4.0)	132.8	0.7 (1.7)	130.8 (4.3)	133.5	26.5 (4.3)	104.3 (5.9)	107.0
Na^+(2BA)	143.3 (3.8)	139.0	0.9 (1.4)	144.2 (4.0)	139.9	28.6 (3.4)	115.6 (5.5)	111.3
Na^+(3HBA)	131.2 (3.1)	135.3	0.7 (1.2)	131.9 (3.3)	136.0	26.2 (3.7)	105.7 (4.9)	109.8
Na^+(4HBA)	131.5 (4.7)	140.9	0.9 (1.3)	132.4 (4.9)	141.8	27.0 (3.6)	105.4 (6.1)	114.8
Na^+(23DHBA)	145.2 (4.1)	149.2	1.3 (1.3)	146.5 (4.3)	150.5	30.6 (3.6)	115.9 (5.6)	119.9
Na^+(24DHBA)	145.3 (3.7)	143.5	0.6 (1.5)	145.9 (4.0)	144.1	28.5 (3.2)	117.4 (5.1)	115.6
Na^+(25DHBA)	145.4 (4.6)	142.4	0.6 (1.5)	146.0 (4.8)	143.0	27.9 (3.2)	118.1 (5.8)	115.1
Na^+(26DHBA)	145.0 (3.7)	147.5	0.7 (1.2)	145.7 (3.9)	148.2	29.4 (3.7)	116.3 (5.4)	118.8
Na^+(34DHBA)	138.0 (3.0)	141.4	0.7 (1.1)	137.9 (3.2)	142.1	24.3 (3.9)	114.4 (5.0)	117.8
Na^+(35DHBA)	136.4 (7.1)	136.4	0.9 (1.1)	137.3 (7.2)	137.3	30.7 (3.9)	106.6 (8.2)	106.6

[a] Uncertainties are listed in parentheses. [b] Density functional theory values from calculations at the B3LYP/6-311+G(2d,2p) level of theory using B3LYP/6-31G* optimized geometries with frequencies scaled by 0.9804.

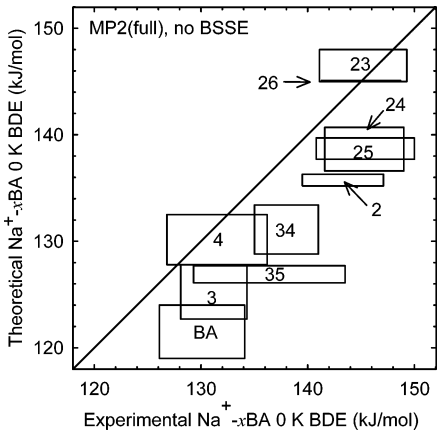

Figure 9. Theoretical MP2(full)6-311+G(2d,2p) versus experimental Na^+-xBA BDEs (in kJ/mol). All values are at 0 K and taken from Table 2. The experimental range corresponds to the measured BDE plus or minus the experimental uncertainty, while the theoretical range corresponds to the calculated BDEs for the ground and low-lying (within ~5 kJ/mol) excited state conformers. The diagonal line indicates the values for which calculated and measured BDEs are equal.

of the Na^+(*x*BA) complexes exist that lie within 10 kJ/mol of the ground state conformation. These species should be able to rapidly interconvert upon association of Na^+ and the *x*BA ligand in our flow tube ion source such that the ion beams generated in our experiments are likely composed of a mixture of low-energy conformations of the Na^+(*x*BA) complexes. Thermalization of these complexes via collisions with the He and Ar bath gases should then provide a Maxwell−Boltzmann distribution of these species. Therefore, the BDEs measured in our experiments should correspond to the most-weakly bound species present in reasonable abundance (i.e., at least a few percent, or within ~5 kJ/mol of the ground state conformation). Thus, in comparing our theoretical and measured BDEs, it is appropriate to include a range of theoretical values corresponding to those of the ground state and the low-energy conformers which may be present and a range of experimental values associated with the measured values and the uncertainties in our measurements. Therefore, the agreement between theory and experiment is illustrated using rectangular boxes, rather than points, in Figures 8 and 9. As can be seen in Figure 8, the agreement between B3LYP theory and experiment is excellent (note the very narrow range of values plotted). The mean absolute deviation (MAD) between the experimental BDEs and those for the ground state conformations calculated at the B3LYP level of theory for all 10 Na^+(*x*BA) complexes is 3.5 ± 2.4 kJ/mol, slightly smaller than the average experimental uncertainty (AEU) of 4.2 ± 1.2 kJ/mol in these measurements. In contrast, MP2 theory does not perform as well and provides BDEs that are systematically lower than the experimental values. The MAD between experiment and MP2 theory is 12.2 ± 3.9 kJ/mol. It has previously been suggested that BSSE corrections overestimate the effects associated with the differing sizes of the basis sets used to calculate the complexes versus the products and can lead to binding energies that are too low, particularly for MP2 theory.[68] Indeed, much better agreement is obtained when BSSE corrections are not included. In this case, the MAD drops to 4.5 ± 2.5 kJ/mol, similar to the AEU of 4.2 ± 1.2 kJ/mol in these measurements.

As discussed above, because multiple low-energy conformers of the Na^+(*x*BA) complexes are likely generated under our experimental conditions, it may be more appropriate to compare the measured BDEs to those calculated for the least stable low-energy Na^+(*x*BA) conformers that are likely to be present in reasonable abundance. In this case, the MAD between the experimental BDEs and B3LYP remains unchanged at 3.5 ± 2.4 kJ/mol because the agreement improves for half of the complexes and degrades for the others. In contrast, the performance of MP2 theory degrades whether or not BSSE corrections are included. The MAD between experiment and MP2 theory becomes 15.6 ± 4.2 kJ/mol when BSSE corrections are included and 6.8 ± 4.5 kJ/mol when BSSE corrections are not included. Therefore, it is somewhat difficult to definitively state that a mixture of conformations is actually accessed in our experiments, but if theory does a reasonable job estimating the relative stabilities of the various conformations of the Na^+-(xBA) complexes and the barriers to interconversion, then a mixture must certainly be present.

As discussed above, the only dissociation pathway observed in the interaction of the Na^+(*x*BA) complexes with Xe corresponds to simple CID to produce Na^+ and the neutral *x*BA ligand. In addition, theoretical calculations find that the binding in these complexes arises from interaction of Na^+ with the lone pair(s) of electrons on the oxygen atoms(s) of the carboxylic acid moiety and/or the hydroxyl substituents. These results suggest that the binding in these complexes is largely electrostatic in nature. Therefore, the strength of the binding in these complexes should be controlled by the nature of the binding interactions, ion−dipole and ion-induced dipole interactions. The effects that the hydroxyl substituent(s) have upon the binding can be examined by comparing the *x*HBA and *x*DHBA ligands to BA. The polarizability of BA is estimated to be 12.91 Å^3 and increases to 13.56 Å^3 upon hydroxyl substitution and to 14.23 Å^3 upon dihydroxyl substitution.[46] The polarizability is not expected to vary significantly with the position(s) or orientations of the hydroxyl substituent(s), and the additivity method we used to estimate these polarizabilities is not sensitive to such structural differences. Therefore, the ion-induced dipole attractions should roughly correlate with the extent of hydroxylation. Indeed, the binding affinity of BA is observed to increase upon hydroxyl substitution in all cases (Table 2). Similarly, the increase in the Na^+-xBA BDE is generally larger for the *x*DHBAs than the *x*HBAs. However, the BDE for the Na^+-(2HBA) complex strongly deviates from this trend, suggesting that other factors are important in determining the binding in these complexes. Ion−dipole interactions should also be important in determining the strength of these complexes. The ion−dipole attractions should correlate with the dipole moments of these ligands. However, the dipole moments of these ligands are very sensitive to the conformation, yet in many cases, very similar theoretical BDEs are found for different conformations/binding geometries. The neutral conformers associated with binding mode A tend to have relatively small dipole moments, and binding occurs via a single interaction with the lone pair of electrons on the carbonyl oxygen atom; however, Na^+ is well aligned to provide good overlap and thus a strong interaction is still achieved. The neutral conformers, associated with binding mode B, tend to have relatively large dipole moments, and binding occurs via a four-membered chelation ring; therefore, the ion−dipole attractions in these complexes should be even more favorable than those for the A conformers. However, this binding geometry is not as ideal for maximal overlap and steric repulsion between the hydroxyl hydrogen atom and the ortho hydrogen atom of the phenyl ring mediates the enhancement in binding associated with dipole and chelation effects. Therefore, in general, the A conformers tend to be more stable than the B conformers except in cases where hydrogen bonding helps

further stabilize the B conformers but is not possible in the A conformers. The neutral conformers, associated with binding mode C, tend to have dipole moments that are intermediate between those of the A and B conformers, but binding occurs via a very favorable six-membered chelation ring. Therefore, the ion−dipole attractions should be more favorable than those for the A and B conformers. Similarly, the neutral conformers, associated with binding mode D, tend to have dipole moments that are similar to those of the C conformers and bind via a five-membered chelation ring. However, interactions with the hydroxyl oxygen atoms are somewhat less favorable than those with the carbonyl oxygen atom. Therefore, the ion−dipole attractions should be somewhat less favorable than those for the C conformers. Indeed, all of the *x*BA ligands that can bind via mode C (i.e., 2HBA, 23DHBA, 24DHBA, 25DHBA, and 26DHBA) exhibit a very similar measured BDE, that is greater than those of ligands that can only bind via mode A, B, or D (i.e., BA, 3HBA, 4HBA, 34DHBA, and 35DHBA) by 6.9−14.9 kJ/mol. In addition, the BDE of 2HBA is observed to increase upon hydroxy substitution in all cases, as expected on the basis of the increased polarizability of these ligands. Likewise, the BDEs of 3HBA and 4HBA are observed to increase upon hydroxy substitution in all cases.

It is interesting that theory suggests that the ground state conformations of Na^+(23DHBA) and Na^+(26DHBA) are not C conformers even though the measured BDEs of these complexes are essentially equal to those for Na^+(24DHBA) and Na^+(25DHBA), whose ground state geometries are C conformers. The additional hydrogen bond stabilization available in the Na^+(23DHBA) and Na^+(26DHBA) complexes makes generally less favorable B and D conformations more favorable than or competitive with the C conformers.

In comparing the BDEs for the ground state conformations of Na^+(3HBA) and Na^+(4HBA), it should be noted that the dipole moments associated with the conformations of the corresponding neutrals are similar, 3.71 versus 3.90 D, respectively (Table 2), while the polarizabilities of these ligands are essentially equal (Figure 1); thus, the ion−dipole and ion-induced dipole attractions should be roughly equivalent in these complexes. Therefore, the Na^+(4HBA) complex likely binds slightly more strongly than the Na^+(3HBA) complex as a result of resonance effects that make the carbonyl oxygen atom more basic and therefore a better binder. In comparing the BDEs of Na^+(34DHBA) and Na^+(35DHBA), it should be noted that the dipole moments associated with the conformations of the corresponding neutrals are much larger for 34DHBA than 35DHBA (i.e., 5.16 versus 3.49 D, respectively, for the ground state complexes), while the polarizabilities of these ligands are essentially equal. In addition, resonance effects in 34DHBA also make the carbonyl oxygen atom more basic and therefore a better binder. As a result, the BDE of Na^+(34DHBA) is greater than that of Na^+(35DHBA). The hydrogen bonding between the hydroxyl substituents possible for 34DHBA, but not for 35DHBA, may also play a role.

The experimental BDEs are also plotted against the estimated polarizabilities of the corresponding neutral ligands in Figure 10. As can be seen in the figure, a roughly linear relationship is observed between the BDEs and the polarizabilities of BA, 3HBA, 4HBA, 34DHBA, and 35DHBA. These results suggest that the polarizability is indeed a considerable factor in determining the strength of binding in the Na^+(*x*BA) complexes. A good linear relationship is also observed between the BDEs and polarizabilities of 2HBA, 23DHBA, 24DHBA, 25DHBA, and 26DHBA, again indicating that the polarizability of these

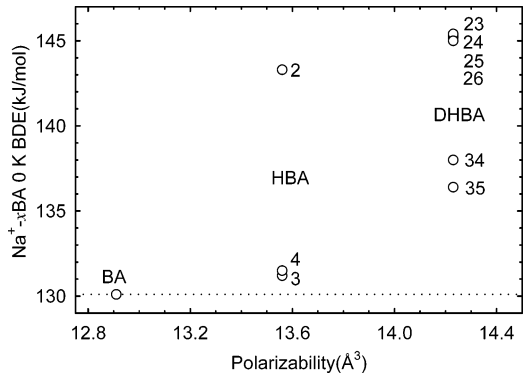

Figure 10. Measured BDEs of Na^+(*x*BA) in kJ/mol versus the estimated polarizability of *x*BA in Å^3.[46]

ligands is an important factor in determining the strength of the binding to Na^+. However, the enhanced stability associated with the larger polarizability of these ligands is overshadowed by the relatively large stabilization gained via six-membered chelation ring formation.

Comparison to Literature Values. We compare our results to those of Zenobi and co-workers who measured the GNa^+B's of a variety of MALDI matrixes, including 25DHBA, using equilibrium and reaction kinetics methods in a Fourier transform ion cyclotron resonance (FT-ICR) mass spectrometer.[23] The equilibrium measurements provided a GNa^+B of 25DHBA of 159 ± 2 kJ/mol, while the reaction kinetics measurements suggest a value of 158 ± 3 kJ/mol. The reaction kinetics value was deemed more reliable because the problem of competing reactions, that is, formation of sodium bound dimers, complicates the direct determination of the equilibrium constant. In any case, both the equilibrium and reaction kinetics GNa^+B's of 25DHBA measured compare well to the value they calculated at the B3LYP/6-31+G* level of theory, 160.1 kJ/mol. To compare these results with those obtained in the present study, the GNa^+B's must be converted to 0 K GNa^+A's (i.e., $\Delta G_{298} \rightarrow \Delta H_0$). Using the thermal corrections determined here, the measured value corresponds to a GNa^+A or BDE of the Na^+(25DHBA) complex of 185 ± 5 kJ/mol, while the calculated value is 187 kJ/mol. In contrast, the BDE of the Na^+(25DHBA) complex measured here is 145.4 ± 4.6 kJ/mol, some 40 kJ/mol or more lower than the value determined by Zenobi and co-workers. Similarly, the value calculated here at the B3LYP/6-311+G(2d,2p)//B3LYP/6-31G* level of theory including ZPE and BSSE corrections is 142.4 kJ/mol, in excellent agreement with our measured value. Thus, the experimental and theoretical work of each research group exhibits good internal agreement; however, the discrepancies between the values reported by Zenobi and co-workers and those determined here are clearly outside of the experimental error of either study.

One possible explanation for the difference in theoretical values was that the basis sets employed by Zenobi and co-workers for geometry optimization and energy calculations differ from those employed in the present study. As detailed in the Supporting Information, Tables 5S and 6S, calculations at the lowest level of theory, 6-31G* for optimization, frequency analysis, energy calculations, and BSSE corrections, provide a BDE of 151.9 kJ/mol, whereas the 6-31+G* and 6-311+G-(2d,2p) basis sets yield BDEs between 142.0 and 143.1 kJ/mol, which are in excellent agreement with the value measured here. Thus, the level of theory cannot explain the discrepancy in theoretical values. We also considered whether the reference base used in the study of Zenobi and co-workers might explain the difference, but it is hard to understand how this could lead

to a 40 kJ/mol difference. Rather, Zenobi and co-workers[24] explain in a later study that the theoretical value reported for the GNa^+B of 25DHBA in the first study assumes that the complex dissociates without a change in conformation of the 25DHBA ligand; that is, dissociation occurs to an excited state asymptote such that the BDE is a diabatic value. Indeed, calculations performed here indicate that this conformation of 25DHBA lies 43.0 kJ/mol higher in energy than the ground state conformation (Supporting Information, Figure 3S). Using the 6-31+G* and 6-311+G(2d,2p) basis sets, we calculate that the diabatic BDE lies between 184.9 and 187.4 kJ/mol, in excellent agreement with the value calculated by Zenobi and co-workers.[23] Thus, the discrepancy in the reported theoretical values is now understood. On the basis of a comparison of the "GNa^+B" measured for 25DHBA and the results of their theoretical calculations, Zenobi and co-workers[24] suggested that 25DHBA does not undergo a change in conformation. This assumption is reasonable for their experimental results because the measured value was determined via proton transfer reaction kinetics/equilibria with a reference base of known GNa^+B chosen such that the difference in GNa^+B's was smaller than the barrier to conformational change of 25DHBA. In contrast, the threshold CID measurements performed here lead to the production of 25DHBA in its ground state conformation because the barrier to conformational change is much smaller than the enthalpy for dissociation to produce Na^+ and 25DHBA. Thus, the present study directly measures the adiabatic BDE. Our results also suggest that the thermochemistry measured by Zenobi and co-workers does indeed correspond to the diabatic value. The adiabatic 0 K GNa^+A's for these *x*BA ligands are given in Table 2, and adiabatic 298 K GNa^+B's, ΔG_{298} values, are reported in Table 3. Recommended values for the adiabatic GNa^+A and GNa^+B of 25DHBA are 145.4 ± 4.6 and 118.1 ± 5.8 kJ/mol, respectively.

It might be argued that the diabatic "GNa^+B's" measured by Zenobi and co-workers are more relevant to understanding and predicting behavior associated with cationization processes that occur in MALDI because cationization occurs via gas phase cation transfer in the MALDI plume and the value they measured was based on cation transfer reaction kinetics/equilibrium. However, their measurements were made at 298 K and in a very low-pressure environment. Additionally, the reference base was chosen to exhibit a similar GNa^+B, a choice necessary as a result of the dynamic range of the FT-ICR instrumentation. In contrast, the temperature and pressure in the MALDI plume are much greater such that the internal energies of the vaporized species should provide sufficient energy to overcome barriers to conformational relaxation of the matrix and analyte molecules.

Implications for MALDI Analyses. The accurate thermochemical data provided by the present study should be useful for the optimization of MALDI analyses. Clearly, the matrix employed for a given MALDI analysis must absorb strongly at the output wavelength of the laser used, typically a N_2 laser with an output wavelength of 337 nm or, somewhat less commonly employed, the fourth harmonic of a Nd:YAG laser with an output wavelength at 266 nm. All of the *x*BA ligands examined here can be used with one or both of these lasers.[35,69−71] Among the *x*BA ligands examined here, 25DHBA has seen the most widespread use because it provides excellent ion signals with a N_2 laser, whereas the performance of several of the other *x*BA ligands with this laser has been rated as fair.[35] However, with the advancing technology, decreasing cost, and growing popularity of other lasers, and the possibility of using one laser for multiple applications, there may be situations where it would be useful to perform MALDI analyses with other lasers. Those appropriate for use with the *x*BA ligands examined here include Ti:sapphire and a variety of eximer lasers (i.e., KCl, KrF, XeF, and XeCl). Assuming that the laser to be employed for a given MALDI analysis can be optimally chosen to match the absorption characteristics of the *x*BA ligands and that sufficient ion signals can be generated, then the choice of which ligand to use would depend on the analyte being examined and whether protonated or cationized analyte is desired. The lower GNa^+A's of BA, 3HBA, 4HBA, 34DHBA, and 35DHBA ligands would tend to lead to greater cationization of the analyte. In contrast, the larger GNa^+A's of 2HBA, 23DHBA, 24DHBA, 25DHBA, and 26DHBA would tend to suppress cationization of the analyte. Clearly, knowledge of the GNa^+A of the analyte molecules to be examined would further facilitate the appropriate choice of matrix.

Conclusions

The kinetic energy dependence of the CID of Na^+(*x*BA), where *x*BA includes benzoic acid and all possible mono- and dihydroxy-substituted benzoic acids, with Xe is examined in a guided ion beam tandem mass spectrometer. The dominant dissociation pathway for all complexes is loss of the intact *x*BA ligand. Thresholds for these processes are determined after consideration of the effects of the reactant kinetic and internal energy distributions, multiple collisions with Xe, and the dissociation lifetime of the collisionally activated complexes. Details of the ground state structures of the neutral *x*BA ligands and Na^+(*x*BA) complexes are determined from ab initio calculations at the B3LYP/6-311+G(2d,2p)//B3LYP/6-31G* and MP2(full)/6-311+G(2d,2p)//B3LYP/6-31G* levels of theory. Very good agreement between the B3LYP theoretically calculated and experimentally determined BDEs was found in most cases. The agreement between MP2 theory and experiment is not quite as good as that found for the B3LYP results, but is still quite reasonable when BSSE corrections are ignored. The trends in the measured BDEs are easy to understand on the basis of the various binding modes, dipole moments, and polarizabilities of these ligands and suggest two very different binding modes of Na^+ to the *x*BA ligands. In contrast, theoretical calculations indicate that there are four very favorable binding modes for Na^+ to these *x*BA ligands. Further, both theoretical and experimental results suggest that ion−dipole and ion-induced dipole attractions are major factors in determining the strength of binding in the Na^+(*x*BA) complexes. The stability of these complexes is greatly enhanced by six-membered chelation ring formation and/or the formation of additional intramolecular hydrogen bonds. The BDEs measured here for the Na^+(*x*BA) complexes suggest that the *x*BA ligands can act as reliable anchors for the sodium cation affinity scale and broaden the range of ligands available as absolute thermochemical anchors. This thermochemical data should be useful for the optimization of MALDI analyses. In addition, this thermochemical data combined with the structural information obtained from the theoretical calculations may provide insight into the ionization processes that occur in MALDI.

Acknowledgment. This work was supported by the National Science Foundation (Grant No. 0518262).

Supporting Information Available: Tables of vibrational frequencies, average vibrational energies at 298 K, and rotational constants of Na^+(*x*BA) and *x*BA in their ground state conforma-

tions, MP2(full)/6-311+G(2d,2p) and B3LYP/6-311+G(2d,2p) energies of all low-energy conformers of Na^+(*x*BA) and ground state conformers of *x*BA, and adiabatic and diabatic BDEs and GNa^+B's for the Na^+(25DHBA) complex calculated at the B3LYP/6-31G*, B3LYP/6-31+G*, and B3LYP/6-311+G(2d,-2p) levels of theory. Figures showing cross sections for CID of Na^+(*x*BA) with Xe, as well as empirical fits to the primary product channels, optimized geometries, dipole moments, and relative energies of all stable conformations of the neutral *x*BA ligands and all low-energy conformers of the Na^+(*x*BA) complexes. This material is available free of charge via the Internet at http://pubs.acs.org.

References and Notes

(1) Tanaka, I. K.; Waki, H.; Ido, Y.; Akita, S.; Yoshida, Y. *Rapid Commun. Mass Spectrom.* **1998**, *2*, 151.

(2) Bahr, U.; Deppe, A.; Karas, M.; Hillenkamp, F.; Giessmann, U. *Anal. Chem.* **1992**, *64*, 2886.

(3) Castro, J. A.; Koster, C.; Wilkins, C. *Rapid. Commun. Mass Spectrom.* **1992**, *6*, 239.

(4) Montaudo, G.; Montaudo, M. S.; Puglisi, C.; Samperi, F. *Rapid Commun. Mass Spectrom.* **1994**, *8*, 1011.

(5) Montaudo, G.; Montaudo, M. S.; Puglisi, C.; Samperi, F. *Anal. Chem.* **1994**, *66*, 4366.

(6) Belu, A. M.; DeSimone, J. M.; Linton, R. W.; Lange, G. W.; Friedman, R. M. *J. Am. Soc. Mass Spectrom.* **1996**, *7*, 11.

(7) Larson, B. S.; Simonsick, W. J., Jr.; McEwen, C. N. *J. Am. Soc. Mass Spectrom.* **1996**, *7*, 287.

(8) Danis, P. O.; Karr, D. E.; Xiong, Y.; Ovens, K. G. *Rapid Commun. Mass Spectrom.* **1996**, *10*, 862.

(9) de Koster, C. G.; Duursma, M. C.; Van Rooij, G. J.; Heeren. R. M. A.; Boon, J. *Rapid Commun. Mass Spectrom.* **1995**, *9*, 957.

(10) Cottrell, J. S.; Koerner, M.; Gerhards, R. *Rapid Commun. Mass Spectrom.* **1995**, *9*, 1562.

(11) Montaudo, G.; Montaudo, M. S.; Puglisi, C.; Samperi, F. *J. Polym. Sci., Part A.: Polym. Chem.* **1996**, *34*, 439.

(12) Blais, J. C.; Turrin, C. O.; Caminade, A. M.; Majoral, J. P. *Anal. Chem.* **2000**, *72*, 5097.

(13) Burton, R. D.; Watson, C. H.; Eyler, J. R.; Lang, G. L.; Powell, D. H.; Avery, M. Y. *Rapid Commun. Mass Spectrom.* **1997**, *11*, 443.

(14) Mormann, M.; Sashir, S.; Derrick, P. J.; Kuck, D. *J. Am. Soc. Mass Spectrom.* **2000**, *11*, 544.

(15) Land. C. M.; Kinsel, G. R. *Abs. Pap. Am. Chem. Soc.* **1998**, *215*, U75.

(16) Steenvoorden, R. J. J. M.; Breuker, K.; Zenobi, R. *Eur. Mass Spectrom.* **1997**, *3*, 339.

(17) Breuker, K.; Knochenmuss, R.; Zenobi, R. *Int. J. Mass Spectrom. Ion Processes* **1999**, *184*, 25.

(18) Breuker, K.; Knochenmuss, R.; Zenobi, R. *J. Am. Soc. Mass Spectrom.* **1999**, *10*, 1111.

(19) Nelson, C, M.; Zhu, L.; Tang, W.; Smith, L. M.; Crellin, K.; Berry, J.; Beauchamp, J. L. *Proceedings of SPIE−The International Society for Optical Engineering* **1996**, *2680*, 247.

(20) Hunter, E. P.; Lias, S. G. *J. Phys. Chem. Ref. Data* **1998**, *27*, 413.

(21) Yassin, F. H.; Marynick, D. S. *Mol. Phys.* **2005**, *103*, 183.

(22) Jørgensen, T. J. D.; Bojesen, G.; Rahbek-Nielsen, H. *Eur. Mass Spectrom.* **1998**, *4*, 39.

(23) Zhang, J.; Knochenmuss, R.; Stevenson, E.; Zenobi, R. *Int. J. Mass Spectrom.* **2002**, *213*, 237.

(24) Zhang, J.; Ha, T. K.; Knochenmuss, R.; Zenobi, *R. J. Phys. Chem. A* **2002**, *106*, 6610.

(25) Wong, C. K. L.; Chan, T.-W. D. *Rapid. Commun. Mass Spectrom.* **1997**, *11*, 517.

(26) Rashidezadeh, H.; Wang. Y.; Guo, B. *Rapid Commun. Mass Spectrom.* **2000**, *14*, 439.

(27) Cheng, H.; Clark, P. A. C.; Hanton, S. D.; Kung, P. *J. Phys. Chem. A* **2000**, *104*, 2647.

(28) Deery, M. J.; Jennings, K. R.; Jasieczek, C. B.; Haddleton, D. M.; Jackson, A. T.; Yates, H. T.; Scrivens, J. H. *Rapid Commun. Mass Spectrom.* **1997**, *3*, 471.

(29) Fujii, T. *Mass Spectrom. Rev.* **2000**, *19*, 111.

(30) North, S.; Okafo, G.; Birrell, H.; Haskins, N.; Camilleri, P. *Rapid. Commun. Mass. Spectrom.* **1997**, *11*, 1635.

(31) Liao, P.-C.; Allison, J. *J. Mass Spectrom.* **1995**, *30*, 408.

(32) Zenobi, R.; Knochenmuss, R. *Mass Spectrom. Rev.* **1998**, *17*, 337

(33) Bauchom, P. J.; Girald, J. E.; Butlar, J.; Belgrader, P. *Anal. Chem.* **1997**, *69*, 4894.

(34) Lehmann, E.; Knochenmuss, R.; Zenobi, R. *Rapid. Commun. Mass. Spectrom.* **1997**, *11*, 1252.

(35) Allwood, D. A.; Dreyfus, R. W.; Perera, I. K.; Dyer, P. E. *Appl. Surf. Sci.* **1997**, *109/110*, 154.

(36) Horneffer, V.; Dreisewerd, K.; Lüdemann, H.-C.; Hillenkamp, F.; Läge, M.; Strupat, K. *Int. J. Mass Spectrom.* **1999**, *185/186/187*, 859.

(37) Horneffer, V.; Reichelt, R.; Strupat, K. *Int. J. Mass Spectrom.* **2003**, *226*, 117.

(38) Štikarovshá, M.; Chmelík, J. *Anal. Chim. Acta* **2004**, *520*, 47.

(39) Mugo, S. M.; Bottaro, C. S. *Rapid Commun. Mass Spectrom.* **2004**, *18*, 2375.

(40) Zhang, Z.; Deng, H.; Deng, Q.; Zhao, S. *Rapid. Commun. Mass Spectrom.* **2004**, *18*, 2146.

(41) Preston-Schaffter, L. M.; Kinsel, G. R.; Russell, D. H. *J. Am. Soc. Mass Spectrom.* **1994**, *5*, 800.

(42) Glückmann, M.; Pfenninger, A.; Krüger, R.; Thierolf, M.; Karas, M.; Horneffer, V.; Hillenkamp, F.; Strupat, K. *Int. J. Mass Spectrom.* **2001**, *210/211*, 121.

(43) Hart, S. R.; Waterfield, M. D.; Burlingame, A. L.; Cramer, R. *J. Am. Soc. Mass Spectrom.* **2002**, *13*, 1042.

(44) Nonami, H.; Fukui, S.; Erra-Balsells, R. *J. Mass Spectrom.* **1997**, *32*, 287.

(45) Chessa, G.; Scrivanti, A.; Seraglia, R.; Traldi, P. *Rapid Commun. Mass Spectrom.* **1998**, *12*, 1533.

(46) Miller, K. J. *J. Am. Chem. Soc.* **1990**, *112*, 8533.

(47) Rodgers, M. T.; Ervin. K. M.; Armentrout, P. B. *J. Chem. Phys.* **1997**, *106*, 4499.

(48) Ervin, K. M.; Armentrout, P. B. *J. Chem. Phys.* **1985**, *83*, 166.

(49) Rodgers, M. T. *J. Phys. Chem. A* **2001**, *105*, 2374.

(50) Teloy, E.; Gerlich, D. *Chem. Phys.* **1974**, *4*, 417.

(51) Gerlich, D. Diplomarbeit, University of Freiburg, Federal Republic of Germany, 1971.

(52) Gerlich, D. In *State-Selected and State-to-State Ion−Molecule Reaction Dynamics, Part I, Experiment*; Ng, C.-Y., Baer, M., Eds.; Advances in Chemical Physics Series; Wiley: New York, 1992; Vol. 82, p 1.

(53) Dalleska, N. F.; Honma, K.; Sunderlin, L. S.; Armentrout. P. B. *J. Am. Chem. Soc.* **1994**, *116*, 3519.

(54) Frisch, M. J.; Trucks, G. W.; Schlegel, H. B.; Scuseria, G. E.; Robb, M. A.; Cheeseman, J. R.; Zakrzewski, V. G.; Montgomery, J. A., Jr.; Stratmann, R. E.; Burant, J. C.; Dapprich, S.; Millam, J. M.; Daniels, A. D.; Kudin, K. N.; Strain, M. C.; Farkas, O.; Tomasi, J.; Barone, V.; Cossi, M.; Cammi, R.; Mennucci, B.; Pomelli, C.; Adamo, C.; Clifford, S.; Ochterski, J.; Petersson, G. A.; Ayala, P. Y.; Cui, Q.; Morokuma, K.; Salvador, P.; Dannenberg, J. J.; Malick, D. K.; Rabuck, A. D.; Raghavachari, K.; Foresman, J. B.; Cioslowski, J.; Ortiz, J. V.; Baboul, A. G.; Stefanov, B. B.; Liu, G.; Liashenko, A.; Piskorz, P.; Komaromi, I.; Gomperts, R.; Martin, R. L.; Fox, D. J.; Keith, T.; Al-Laham, M. A.; Peng, C. Y.; Nanayakkara, A.; Challacombe, M.; Gill, P. M. W.; Johnson, B.; Chen, W.; Wong, M. W.; Andres, J. L.; Gonzales, C.; Head-Gordon, M.; Replogle, E. S.; Pople, J. A. *Gaussian 98*, revision A.11; Gaussian, Inc.: Pittsburgh, PA, 2001.

(55) Foresman, J. B.; Frisch, Æ. *Exploring Chemistry with Electronic Structure Methods*, 2nd ed.; Gaussian, Inc.: Pittsburgh, PA, 1996.

(56) Muntean, F.; Armentrout, P. B. *J. Chem. Phys.* **2001**, *115*, 1213.

(57) Beyer, T. S.; Swinehart, D. F. *Commun. ACM* **1973**, *16*, 379.

(58) Stein, S. E.; Rabinovitch, B. S. *J. Chem. Phys.* **1973**, *58*, 2438.

(59) Stein, S. E.; Rabinovitch, B. S. *Chem. Phys. Lett.* **1977**, *49*, 183.

(60) Pople, J. A.; Schlegel, H. B.; Ragavachari, K.; De Frees, D. J.; Binkley, J. F.; Frisch, M. J.; Whitesides, R. F.; Hout, R. F.; Hehre, W. J. *Int. J. Quantum Chem. Symp.* **1981**, *15*, 269.

(61) De Frees, D. J.; McLean, A. D. *J. Chem. Phys.* **1985**, *82*, 333.

(62) Khan, F. A.; Clemmer, D. E.; Schultz, R. H.; Armentrout, P. B. *J. Phys. Chem.* **1993**, *97*, 7978.

(63) Chesnavich, W. J.; Bowers, M. T. *J. Phys. Chem.* **1979**, *83*, 900.

(64) See, for example, Figure 1 in Dalleska, N. F.; Honma, K.; Armentrout, P. B. *J. Am. Chem. Soc.* **1993**, *115*, 12125.

(65) Armentrout, P. B. In *Advances in Gas-Phase Ion Chemistry*; Adams, N. G., Babcock, L. M., Eds.; JAI: Greenwich, CT, 1992; Vol. 1, pp 83−119.

(66) Armentrout, P. B.; Simons, J. *J. Am. Chem. Soc.* **1992**, *114*, 8627.

(67) Rodgers, M. T.; Armentrout, P. B. *J. Phys. Chem. A* **1997**, *101*, 2614.

(68) Feller, D. *Chem. Phys. Lett.* **2000**, *322*, 543.

(69) Dearden, J. C.; Forbes, W. F. *Can. J. Chem.* **1959**, *37*, 1294.

(70) Kamath, V.; Mehta, J. D.; Bafna, S. L. *Appl. Chem. Biotechnol.* **1975**, *25*, 743.

(71) Baum, J. C.; McClure, D. S. *J. Am. Chem. Soc.* **1979**, *101*, 2335.